

Atomistic study of the interaction between a microcrack and a hard inclusion in β -SiC

A. Mattoni and L. Colombo*

INFN-SLACS Sardinian Laboratory for Computational Materials Science and Dipartimento di Fisica Università di Cagliari, Cittadella Universitaria, I-09042 Monserrato (Ca), Italy

F. Cleri

ENEA, Unità Materiali e Nuove Tecnologie, and INFN Centro Ricerche della Casaccia, CP 2400, I-00100 Roma, Italy

(Received 5 April 2004; published 17 September 2004)

We present an atomistic investigation on mechanical loading effects in a model fiber-reinforced β -SiC monocrystal where a crack is present. Our simulations are both consistent with the basic results of elementary continuum mechanics and provide a deeper physical insight at the nanoscale. In particular, we propose an effective renormalization of some basic quantity (e.g., the crack length), which reconcile continuum theory to atomistics. Finally, we prove that the interaction between the microcrack and the hard inclusion (fiber) is able to increase the strength of the β -SiC lattice and falls beyond the linear regime. We consistently provide a corresponding constitutive equation for the total stress field for an interacting crack-fiber pair.

DOI: 10.1103/PhysRevB.70.094108

PACS number(s): 62.20.Mk, 61.72.Bb, 81.40.Jj

I. INTRODUCTION

High hardness, low density and high inertness—among other interesting properties—make ceramic materials very promising (and, therefore, quite extensively investigated) for structural applications. There are, however, two basic features severely limiting their straightforward use, namely, their brittle nature as well as their reduced-fracture toughness. In other words, a possible crack front can propagate quite easily (once generated) and affect the overall mechanical reliability of a given structure.

A possible improvement toward an increased fracture toughness has been proposed to be fiber reinforcement. It basically consists in the incorporation of suitable fibers into a ceramic matrix. There are at least two toughening mechanisms ruled out by fibers, namely, crack deflection and fiber bridging.¹ While such mechanisms have been reasonably well developed as technological materials processing tools, there is still a lack of knowledge about the interaction features between a crack tip and a matrix-fiber interface at the most fundamental, i.e., atomistic length scale.

There are serious conceptual and computational limitations in applying continuum mechanics (i.e., the standard theoretical framework for structural engineering) to the above situation. Stress and strain fields computed by continuum theories at vanishing distance from the crack tip become mathematically singular,² thus preventing any meaningful prediction of mechanical properties (e.g., toughness or crack deflection) in the near vicinity of the crack tip. In other words it is difficult to project the continuum approach at the length scale where a direct interaction between the fracture event and the phase boundary between the fiber and the matrix occurs. Furthermore, the corresponding total computational workload of a continuum analysis based on finite elements would be prohibitively large for the extreme refinement of the numerical mesh requested by the local nonhomogeneity of the system at such a short length scale. Typically, the mesh refinement would indeed be stopped at a longer scale, representing a possibly bad coarse-grained pic-

ture of the actual micro- or nanoscale structure of the fiber-reinforced system.

In this work we present an atomistic investigation based on model-potential molecular dynamics (MD) simulations on mechanical loading effects in a model fiber-reinforced β -SiC monocrystal where a crack is present. The fiber is actually modeled as a cylindrical diamond nanofiber, corresponding to the case of a hard inclusion. Silicon carbide is, in turn, selected as the prototypical covalently bonded ceramic of great potential interest as candidate composite material for aerospace applications. In the present work the material is resolved atomistically, so that there is no ambiguity in representing its actual structure displaying an elastic nonhomogeneity at the nanoscale. In other words, present simulations will naturally operate at the length scale, which falls out-of-reach of continuum theories. MD simulations, such as the present one, are well-established tools used to investigate the mechanics and fracture of materials.^{3,4} Since the system response is here computed by the collective displacement of atoms, the resulting mechanical behavior is governed by the selected interatomic potential that, in turn, is derived from a fundamental understanding of chemical bonding between atoms. The selection of suitable constitutive equations for the mechanical behavior is therefore not needed as in continuum mechanics.

The main goal of the present investigation is twofold: on the one side, we want to understand whether linear elastic fracture mechanics and atomistic simulations do provide similar pictures for the stress field of such a system; on the other side, we aim at getting an improved physical insight on the interaction between a crack tip and a hard elastic inclusion (fiber) by using atomistic simulations as virtual laboratory.

The paper is organized as follows. In Sec. II we describe the present computational framework, taking special care in describing the geometry and the border conditions. In Sec. III we present our results for the two isolated defects (the crack and the inclusion) and for an interacting crack-inclusion pair. We extensively discuss present results with

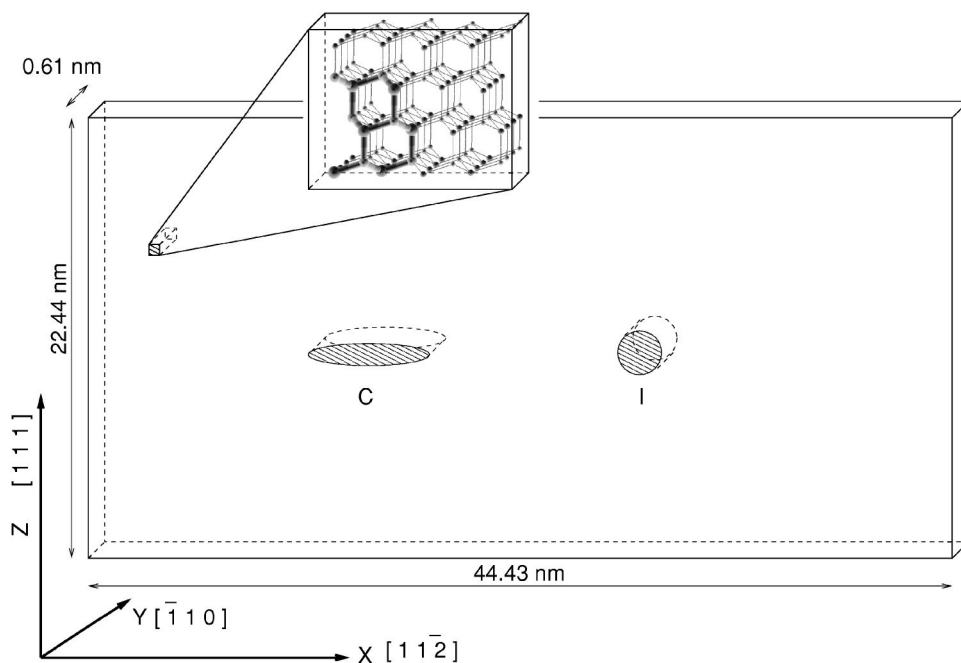


FIG. 1. Geometry, orientation, crystal structure, and dimension of the simulation cell. Both the crack (C) and the cylindrical inclusion (I) are shown as well.

respect to the prediction of linear elastic fracture mechanics and we provide an important renormalization concept. Finally, we prove that the phenomena investigated here fall beyond the linear response regime and, by means of atomistic simulations, we provide a constitutive model for the non-linear interaction between the crack tip and the model fiber.

II. COMPUTATIONAL FRAMEWORK

The typical simulation cell (see Fig. 1) was a thin slab containing 60 480 atoms of a SiC monocystal with zincblend structure (β -SiC). Atoms were arranged in a periodic supercell made of $84 \times 2 \times 30$ unit cells containing 12 atoms each, resulting in a system with dimensions $444.28 \times 6.107 \times 224.37 \text{ \AA}^3$. The x , y , and z axes of the system were aligned along the $[11\bar{2}]$, $[\bar{1}10]$, and $[111]$ orthogonal directions, respectively. In the x - y plane the system was kept fixed at the equilibrium lattice parameter of β -SiC (4.318 \AA) and periodically repeated. In the z direction the crystal was elongated in steps up to a tensile strain of 8% by means of the constant traction method.⁵ According to this method, periodic boundary conditions were removed along the z direction and the resulting surfaces (in our case one top silicon and one bottom carbon (111) shuffle planes) were subject to constant forces (tractions) to mimic the embedding into an infinite bulk at the same level of strain. As a consequence, the top and the bottom surfaces are subject to opposite net forces of modulus 3.72 eV \AA^{-1} per unit area of 16.15 \AA^2 (calculated according to the Tersoff potential⁶), and corresponding to a stress $0.23 \text{ eV \AA}^{-3} = 36.84 \text{ GPa}$ (i.e., about 6.6% of the Young's modulus along the $[111]$ direction). The typical loading condition adopted here consists of fixed stress along z direction $\sigma_{zz} = \sigma_{zz}^\infty$ and fixed strain in the orthogonal plane $\epsilon_{xx} = \epsilon_{yy} = 0$, and therefore, represents the plane-strain border condition of continuum mechanics.²

At least three different interatomic potentials for SiC have been introduced thus far.⁶⁻⁸ Our simulations are based on the bond-order potential developed by Tersoff,⁶ which has been widely applied to study the structural, mechanical,⁹ thermal, vibrational, and surface properties of β -SiC.¹⁰ In particular, the thermomechanical bulk properties of silicon carbide calculated according to present model¹⁰ are in good agreement with experimental or *ab initio* data.¹¹ Furthermore, the Tersoff potential is able to reproduce the brittle failure of silicon carbide under tensile load.¹²⁻¹⁴ A modification of Tersoff potential has indeed been proposed by Tang *et al.*,⁹ consisting of scaling the original interaction cutoff upon the actual global deformation. Nonetheless, the present calculations are based on the original form of the potential for two reasons: (i) the modification does not apply to nonhomogenous systems containing cracks and inclusions, (ii) we are interested in tensile-strained system at $T=0 \text{ K}$ in which case the modification is less relevant.

Two kinds of defects were studied in the present work, namely a microcrack and an inclusion. To find their equilibrium configurations in the bulk monocystal we first performed a series of structural relaxations by a standard damped dynamics method. The convergence was controlled by monitoring the maximum atomic force and stress components, and the system was considered fully relaxed for atomic forces below 0.01 eV \AA^{-1} . The $\sigma_{\alpha\beta}$ stress tensor of a system at $T=0 \text{ K}$ is in principle defined as

$$\sigma_{\alpha\beta} = \frac{1}{V} \frac{\partial U}{\partial \epsilon_{\alpha\beta}} \quad (1)$$

where U is the internal energy of the system and $\epsilon_{\alpha\beta}$ is the strain tensor for the Cartesian coordinates α and β .¹⁵ Within the Tersoff force model it is possible to cast the internal energy U of the system into a sum of single-site energies v_i

$$U = \sum_i v_i = \sum_i \left\{ \sum_j [V_R(r_{ij}) - b_{ij} V_A(r_{ij})] \right\}, \quad (2)$$

where i and j label atoms, r_{ij} is the distance between atom i and j , $b_{ij}=f[\zeta]$ is the Tersoff bond-order functional with $\zeta = \sum_{k \neq i,j} g(r_{ij}, r_{ik})$. In Eq. (2) V_R represents the two-body repulsive potential, while V_A is the two-body attractive one.⁶ By means of Eqs. (1) and (2) we easily get an expression for the $\sigma_{\alpha\beta}$ in terms of atomic stresses $\sigma_{\alpha\beta,i}$

$$\sigma_{\alpha\beta} = \frac{1}{N} \sum_i \left(\frac{V}{N} \right)^{-1} \frac{\partial v_i}{\partial \epsilon_{\alpha\beta}} = \frac{1}{N} \sum_i \sigma_{\alpha\beta,i}, \quad (3)$$

once we attribute to any atom the same volume V/N . Such an attribution is in principle correct for homogeneous systems only; nonetheless, we adopt the definition given in Eq. (3) even in the present investigation where cracks and inhomogeneities are found. We heuristically prove the reliability of this assumption by verifying that the resulting atomistic data agree with the elastic continuum theory (see Sec. III). Furthermore, we remark that a similar approach was successfully applied by Cleri *et al.*¹⁶ for the case of a crack tip in metal.

For any pair i - j of interacting atoms we calculate the average atomic stress $1/2(\sigma_{\alpha\beta,i} + \sigma_{\alpha\beta,j})$ and we attribute it to the average atomic position of the selected i - j atom pair. We will refer to such a quantity as the local stress tensor $\bar{\sigma}_{\alpha\beta}(x, y, z)$. For the present plane strain condition the y direction is not relevant, therefore, we can average

$$\sigma_{\alpha\beta}(x, z) = \frac{1}{L_y} \int_0^{L_y} \bar{\sigma}_{\alpha\beta}(x, y, z) dy, \quad (4)$$

and accordingly define the stress $\sigma_{\alpha\beta}(x, z)$ in x - z plane. In the following we will focus our investigation on such plane-averaged stress tensor $\sigma_{\alpha\beta}(x, z)$.

III. RESULTS

A. Isolated crack in silicon carbide

First of all we studied a stable microcrack in strained β -SiC monocrystal. To insert the microcrack we cut a number of bonds across the shuffle (111) plane in a perfect β -SiC monocrystal homogeneously strained at 8% in the z direction, similarly to the procedure described by Cleri *et al.*¹⁶ This direction has been chosen since the (111) shuffle surface in β -SiC is that of minimum energy¹⁰ and, therefore, a crack in the (111) shuffle plane is the most likely to occur. The front of the crack is parallel to the y axes (see Fig. 1) and, due to the periodic boundary conditions along the y direction, it extends through the whole sample. The half length a of the microcrack measured along the x direction is about 18 Å [the uncertainty in the measurement of a is related to the atomic resolution and corresponds to the distance between two adjacent (11 $\bar{2}$) planes]. In response to the applied load the microcrack turns into an elliptical Griffith-like hole.¹⁷ However, for the given geometry and loading conditions no crack propagation is observed during any of the simulations. This feature is not an artifact; rather, we selected those conditions to ensure stability.¹⁸

A map of the stress $\sigma_{zz}(x, z)$ in the x - z plane is represented in Fig. 2 for a fully relaxed configuration at 8% strain. Different tones of gray represent the tensile (light gray) and compressive (dark gray) stress, respectively. The terms tensile and compressive are referred to the asymptotic stress value σ_{zz}^∞ (mid-gray tone at the left and right extreme of Fig. 2). We first point out that numerical data qualitatively exhibit the stress enhancement at the crack tip as expected from elementary theory of linear elastic fracture mechanics (LEFM).² Figure 2 shows that the present atomistic simulation correctly predicts the formation of two tensile lobes that extend outward from the crack tips. This feature is clearly shown by the bottom panel of Fig. 2, where isostress contour plots are reported. On the contrary, along the edges of the cut, two compressive lobes are formed.

Let us now move to a more quantitative study of the crack-induced stress field. Let (X_C, Z_C) be the coordinates of the center of the crack. We calculated the stress along a horizontal line for values $x > X_C$ and $z = Z_C$. The corresponding stress $\sigma_{zz}(X)$ data are represented as open circles in Fig. 3 as function of reduced units $X = (x - X_C)/a$. The asymptotic behavior of $\sigma_{zz}(X)$ for both $X \rightarrow 1$ and $X \rightarrow \infty$ are nicely fitted by a function $A(X - B)^D + C$. We find, however, that two different exponents D are necessary to describe the whole set of data. In the near vicinity of the crack tip ($1 < X < 4$), the stress diverges as the inverse of the square root of the distance ($D \sim -0.5$). The fitting curve is represented as a continuous line in Fig. 3 and is unable to fit data at a distance greater than $X = 4$. As the distance from the crack tip increases ($X > 4$), the σ_{zz} stress decays according to a different power law with exponent $D \sim -2$. The fit is represented in Fig. 3 as a dashed line. Far away from the crack tip the asymptotic value of the stress σ_{zz} tends to the external applied load $\sigma_{zz}^\infty = 0.23 \text{ eV \AA}^{-3}$.

According to LEFM, the stress field produced by a sharp crack the under the remote load σ_{zz}^∞ and contained in a large plate of length $2a$ was calculated by Inglis in Ref. 2 to be

$$\sigma_{zz}(x) = \sigma_{zz}^\infty \frac{X}{\sqrt{X^2 - 1}} \sim \begin{cases} \frac{1}{\sqrt{2(X-1)}} & \text{when } X = \frac{x - X_C}{a} \rightarrow 1^+ \\ \sigma_{zz}^\infty \left(1 + \frac{1}{2X^2} \right) & \text{when } X = \frac{x - X_C}{a} \rightarrow \infty \end{cases}, \quad (5)$$

where the relevant asymptotic trends are explicitly reported on the right terms. We conclude that the atomistic simulations correctly reproduce the asymptotic far and near-field power laws predicted by LEFM.

In order to test the quantitative agreement between the atomistic data and the Inglis formula, we plot in Fig. 4 the quantity $\Sigma = \sigma_{zz}(X) \sqrt{X^2 - 1} / \sigma_{zz}^\infty$ as a function of X . According to Eq. (5) we expect a straight line, as indeed proved by Fig. 4 up to a distance of about 200 Å. Such an excellent agreement stands for the reliability of the present atomistic simulation and, in particular, of Eq. (3). Nevertheless, Fig. 4 de-

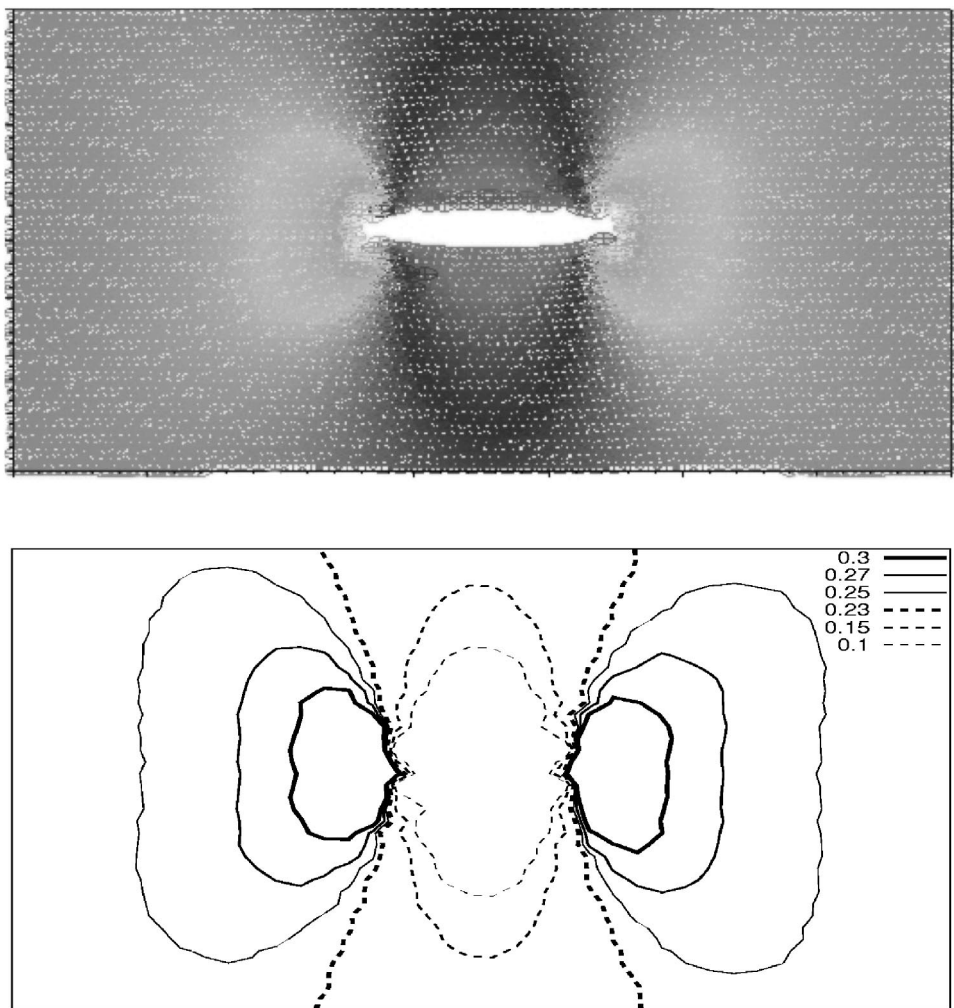


FIG. 2. Top panel: stress map $\sigma_{zz}(x, z)$ of a stable crack of semi-length $a=18 \text{ \AA}$ in strained β -SiC. The applied tensile strain is $\varepsilon_{zz}=8\%$. Light gray represents tensile stress, dark gray represents compressive stress. Bottom panel: isostress contour plot (units of eV \AA^{-3}) for the same crack. We clearly observe the formation of a stress dipole, with enhanced stress at the two crack tips. Note that only a small portion of the simulation cell is represented for sake of clarity. Such a portion corresponds to a length of 14 nm and 8 nm in the x and z directions, respectively.

serves a more detailed analysis. In order to match LEFM equations to atomistics it is necessary to introduce an effective semilength of the crack a (27 \AA) that does not correspond to the actual dimension of the cut (that we remark was as small as 18 \AA). We found that the effective length corresponds approximately to the sum of the real length to the extension of the region where the local stress is higher than 0.3 eV/\AA^{-3} . At such stress values β -SiC mechanical response is strongly nonlinear. A possible origin for such a discrepancy could be attributed to our definition of stress that does not take into account local volume deformation and attributes the same local volume to each atom [see Eq. (1)]. However in the near vicinity of the crack, bonds are elongated and atomic volumes are expanded; this correction, in turn, would reduce the stress at the crack tip, and the difference between the actual dimension of the crack and the effective parameter would accordingly increase. Furthermore, the discrepancy would be stronger at the crack tip and would vanish far from it. In conclusion, we exclude artifacts in our stress definition. On the other hand, we remark that some approximations, as follows, are present in LEFM: (i) the crack is assumed sharp, as the limiting configuration of an elliptic hole when the shorter half axis approaches zero; (ii) the crack faces are traction free; and (iii) linearity is assumed everywhere. None of these assumptions is indeed verified at

the atomic level. This is a source of conceptual difference between continuum and discrete analysis, and we propose this latter to be more physically sound. In any case, by means of Fig. 4 we can state that, although some (or even any) basic assumption of LEFM is not strictly fulfilled, we can reconcile atomistics with continuum analysis by a proper renormalization of the crack length.

B. Isolated diamond inclusion in silicon carbide

As a prototype of a hard inclusion we consider the case a diamond fiber inserted into a β -SiC matrix as a pure chemical defect with no bond reconstruction or buckling at the interface (i.e., coherent with the crystalline matrix). This assumption is validated by recent experimental results of Pecz *et al.*¹⁹ where, by implanting carbon atoms in β -SiC at high temperature, the formation of coherent diamond inclusions with size of about $\sim 3 \text{ nm}$ was shown. We selected a cylindrical region whose axis is parallel to the y coordinate and with radius $R=1 \text{ nm}$. We then replaced the atoms of the cylindrical portion of the crystal by the same number of carbon atoms to represent the cross-section of an infinite fiber along the y direction. Because the C-C bond is 12% smaller than the Si-C bond, the inclusion gives rise to a sizeable deformation field in the SiC matrix that, at variance with the crack

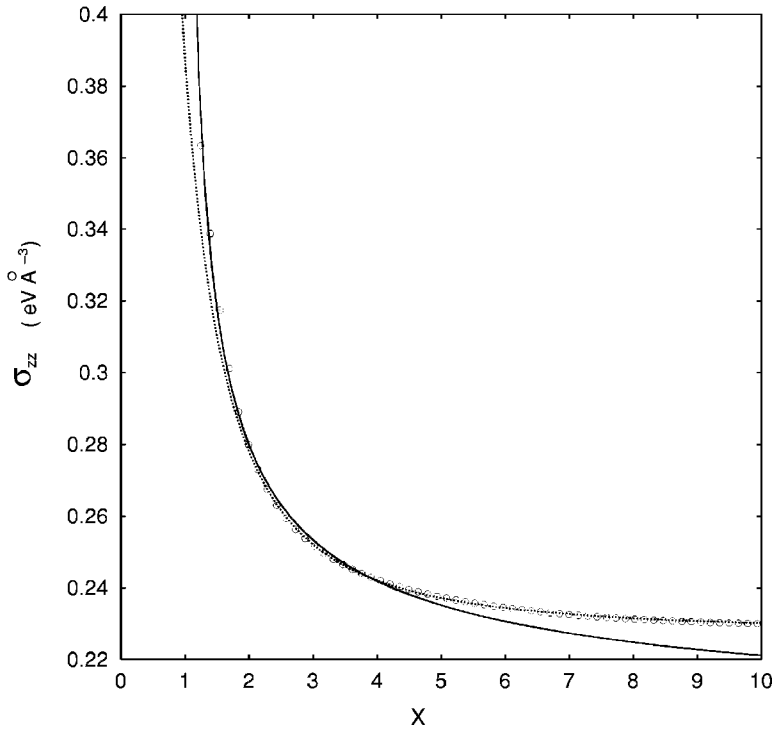


FIG. 3. Stress component $\sigma_{zz}(X)$ as a function of the distance X from the crack tip in reduced units $X=(x-X_C)/a$, open circles represent atomistic data, continuous line represents a $\sim X^{-0.5}$ trend, while dashed line represent the $\sim X^{-2}$ behavior.

case, can be studied without applying any load. A map of the stress field $\sigma_{zz}(x, z)$ for the unstrained β -SiC monocrystal ($\epsilon_{zz}=0$) is represented in Fig. 5. Light gray corresponds to high tensile stress. It is worth noting that the stress field close to the carbon inclusion has a quadrupole shape; the top and bottom lobes are regions of tensile stress because along the [111] direction the softer Si-C bonds of the host matrix are pulled by the stronger C-C bonds of the inclusion. The right and left lobes of the β -SiC matrix undergo to compressive stress because there the local Si-C bonds are shortened to match the C-C bonds of diamond inclusion (see also Fig. 5, bottom panel for the corresponding isostress contour plots). The total stress induced in the matrix increases with the radius R of the inclusion. It has been proved that when a critical radius is reached, the formation of lattice damage at the interface (amorphization at the interface) is energetically

favored.¹⁹ The critical radius is, moreover, expected to decrease if an external load is applied. Our calculations prove that, in agreement with the experimental findings, a coherent 2 nm large inclusion under a strain of 8 % is stable, i.e., no defects are formed at the matrix/inclusion border.

As for the displacement field $u(z)$, we consider an inclusion in an unstrained β -SiC sample. Let z_i be the coordinate of a given i th atom for a perfect β -SiC monocrystal. Let z'_i be the coordinate of the same atom when the diamond inclusion is present and forces have been fully relaxed. Finally, let (X_I, Z_I) be the coordinate of center of the circular section corresponding to the inclusion. We measure the atomic displacement field $u_z(z_i) = z'_i - z_i$ along a vertical line ($x = X_I$ and $z > Z_I$) starting at the center of the inclusion; the distance is measured in reduced units $Z = (z - Z_I)/R$. The results of such calculations are reported in Fig. 6 as open circles. It can be

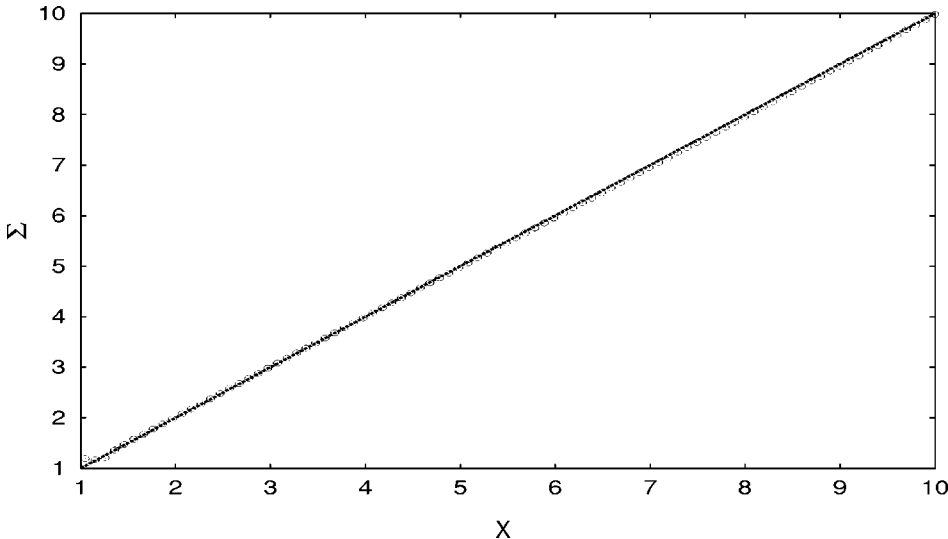


FIG. 4. Plot of the $\Sigma = \sigma_{zz}(X) / \sigma_{zz}^\infty \sqrt{X^2 - 1}$ function distance from the crack tip in reduced units $X=(x-X_C)/a$. Full line: theoretical LEFM prediction; open circles: present atomistic data.

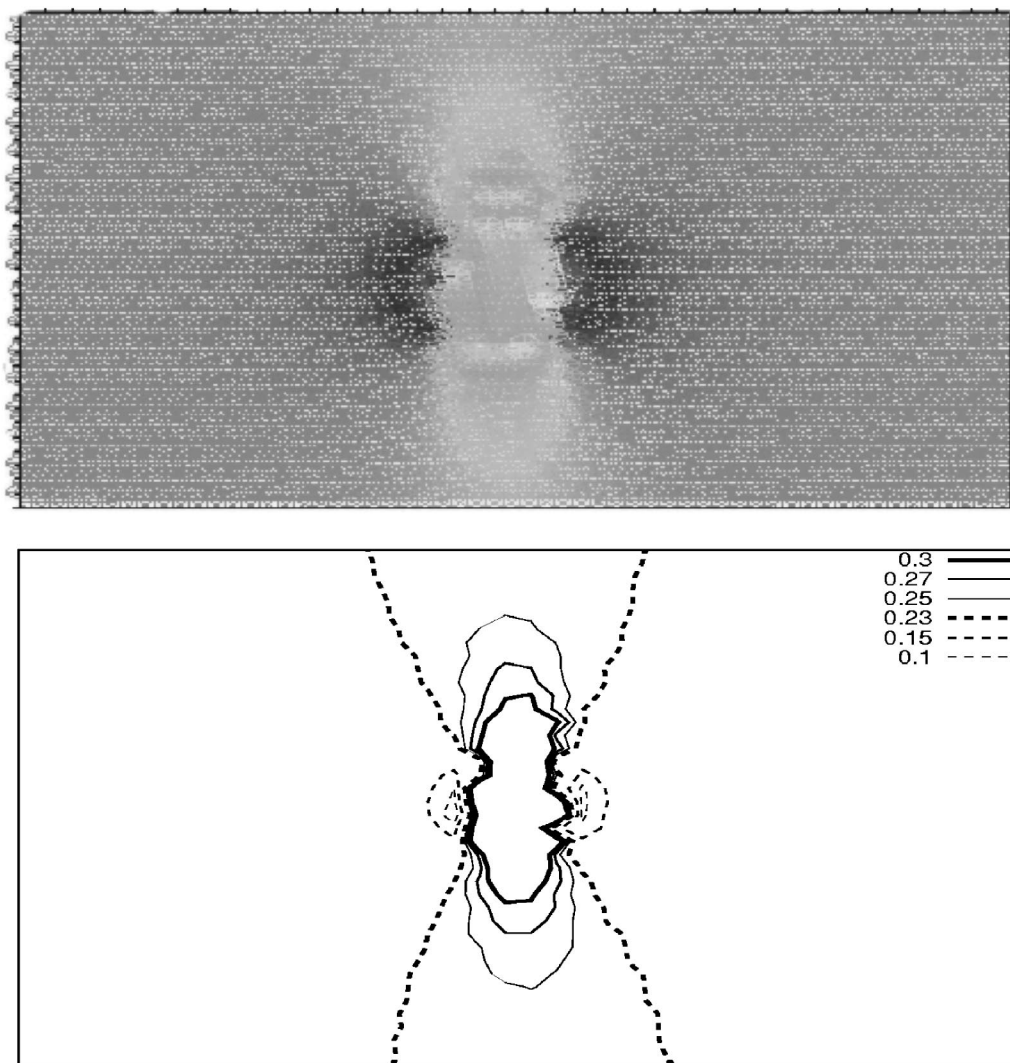


FIG. 5. Top panel: stress map $\sigma_{zz}(x, z)$ of β -SiC containing a diamond inclusion ($a=10 \text{ \AA}$). Bottom panel: isostress contour plot (units of eV \AA^{-3}) for the same inclusion. We clearly observe the formation of a quadrupole structure with tensile stress enhanced at the top and bottom lobes and depleted at the left and right lobes. Note that only a small portion of the simulation cell is represented for the sake of clarity. Such a portion corresponds to a length of 14 nm and 8 nm in the x and z directions, respectively.

pointed out that the displacement is a decreasing function of the distance, as expected. In order to find out the decaying behavior, data are fitted by the $A(Z-B)^C+D$ function of the distance, obtaining a power law with exponent $C \sim -1$. This result is nicely in agreement with the theory of elasticity in the case of a spherical elastic inclusion in a homogeneous medium. According to Eshelby²⁰ the displacement decreases asymptotically as the inverse square of the distance $\sim 1/Z^2$. For an infinite fiber, similarly to the electrostatic case of a spherical point charge versus an infinite charged line, the asymptotic decrease has a different power law due to the different dimensionality and corresponds, in fact, to the inverse of the distance $\sim 1/Z$.

C. Interaction between a microcrack and a hard inclusion in silicon carbide

In order to study the interaction between the microcrack and the inclusion, we performed several calculations in

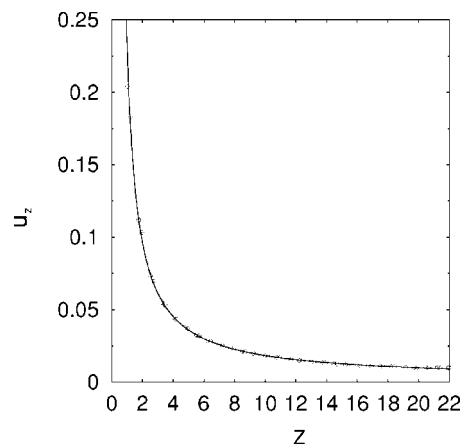


FIG. 6. Atomic displacement $u_z(Z)$ (units of equilibrium β -SiC lattice constant 4.32 \AA) as a function of the distance from the inclusion, measured in reduced units $Z=(z-Z_I)/R$. Open squares: atomistic data; dashed line: fitting curve $\sim Z^{-1}$.

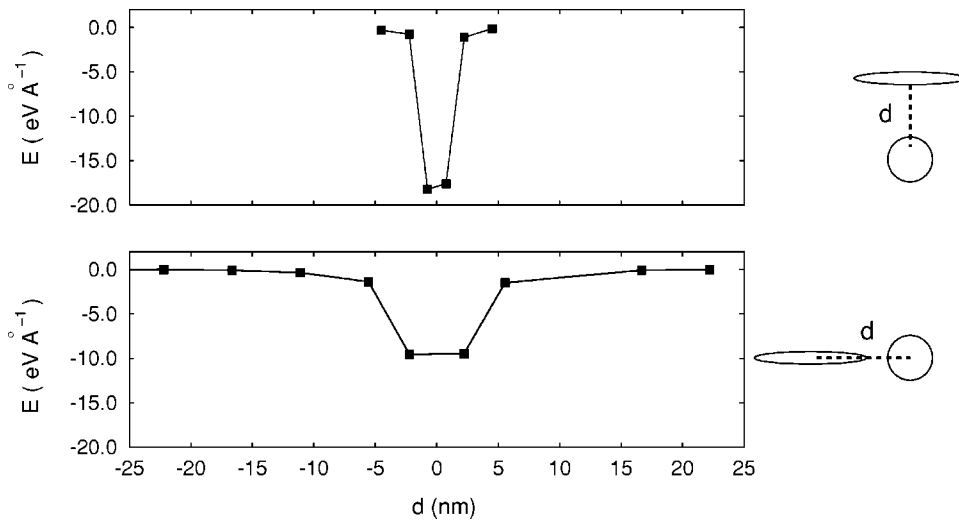


FIG. 7. Top panel: energy of strained β -SiC ($\epsilon_{zz}=8\%$) containing a stable crack and a diamond inclusion as a function of the relative distance for a vertical crack-inclusion alignment; bottom panel: the same for horizontal alignment.

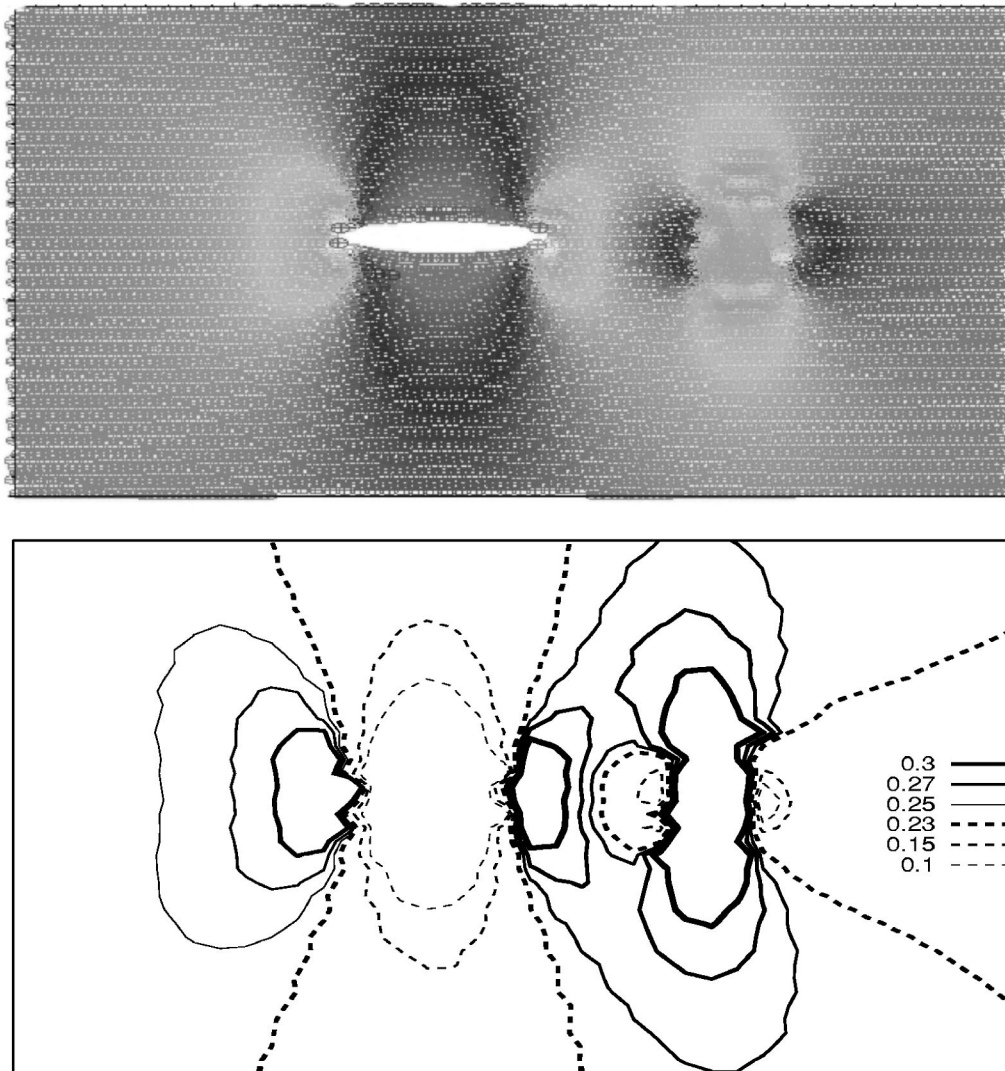


FIG. 8. Top panel: stress map $\sigma_{zz}(x,y)$ of β -SiC containing both a diamond inclusion ($R=10 \text{ \AA}$) and a stable crack ($a=18 \text{ \AA}$) at the distance of 5.5 nm. Bottom panel: isostress contour plot (units of eV \AA^{-3}) for the same system. Note that only a small portion of the simulation cell is represented for the sake of clarity. Such a portion corresponds to a length of 18 nm and 10 nm in the x and z directions, respectively.

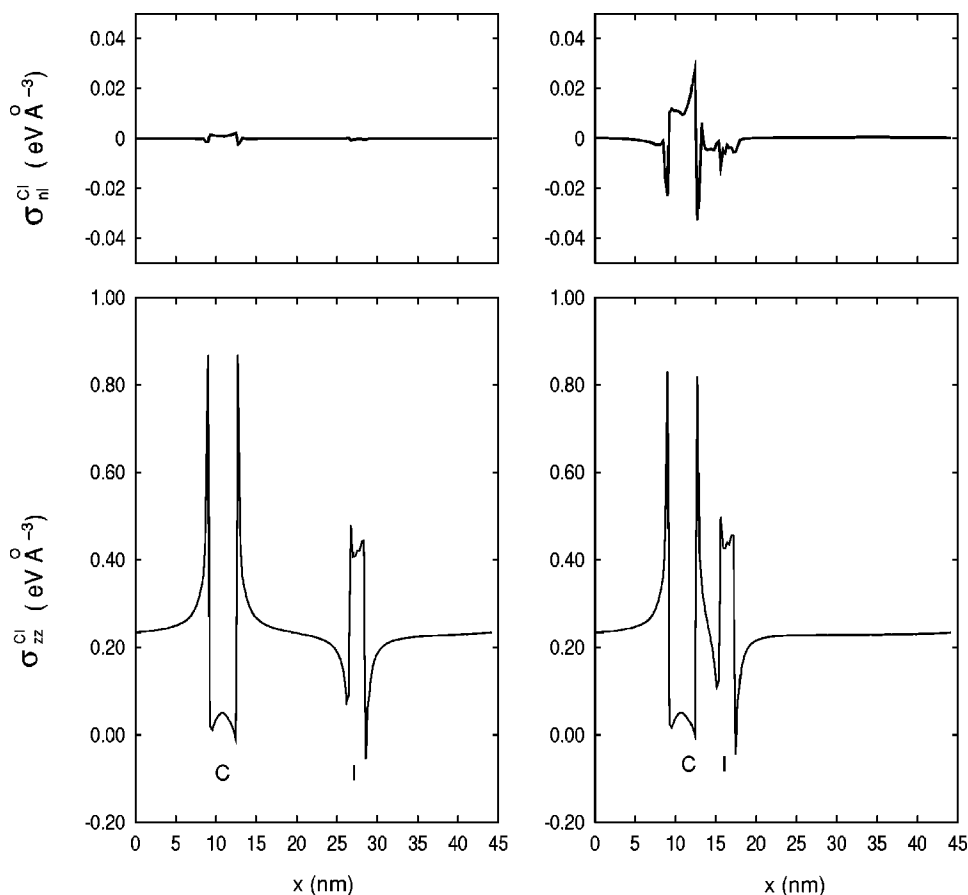


FIG. 9. Bottom panels: stress component $\sigma_{zz}^{CI}(x)$ along the line connecting the crack tip to the inclusion, when their distance is ~ 15 nm (left) and ~ 5.5 nm (right). Top panels: corresponding defect of linearity σ_{nl}^{CI} of the stress field.

which we varied the relative distance between the two defects. The distance is measured with respect to the defect centers (X_C, Z_C) and (X_I, Z_I) . The starting point for any run was a β -SiC monocrystal containing the carbon inclusion relaxed at zero load. The system was then strained by the application of constant tractions (corresponding to 8% of tensile strain in perfect β -SiC) and again fully relaxed. At this stage the crack was inserted into the system as explained above. We inserted the microcrack always in a (111) shuffle plane, at different distances from the inclusion, along two different alignments: in the case of horizontal alignment (hereafter referred to as H) the microcrack was put at different distances along the horizontal line $(x, z=Z_I)$ as indicated in Fig. 7 (bottom); in vertical alignment geometry (hereafter referred to as V) the distance was varied along the vertical line $(x=X_I, z)$ as indicated in Fig. 7 (top). The energy of a system containing both the inclusion and the microcrack is reported in the same figure for both alignments. Being the inclusion an infinite fiber, our result is expressed as energy per unit length of fiber.

Let us first consider case H. As the distance between the microcrack and inclusion decreases, the energy of the system lowers. This result indicates that there exists an attraction basin between the two objects. As no bond rearrangement occurs (the defects are spatially separated at all the distances considered), we can further conclude that such an energy basin has to be attributed to the interaction between the stress fields of the microcrack and of the hard inclusion. When the relative distance of the two defects is about 5.5 nm, opposite

stress lobes interact with an energy gain $\Delta E \sim 1.5 \text{ eV } \text{\AA}^{-1}$. The relative map of the stress is represented in Fig. 8; the region corresponding to the highest tensile stress (delimited by the isostress contour $\sigma_{zz}=0.27 \text{ eV } \text{\AA}^{-3}$, as indicated in Fig. 8, bottom panel) at the right crack tip is made smaller by the compressive lobe of the inclusion. At the same time, the isostress contour $\sigma_{zz}=0.25 \text{ eV } \text{\AA}^{-3}$ (corresponding to a lower value of tensile stress) turns out to be extended all around the inclusion. The maximum depth of the attraction basin is reached when the crack tip and the inclusion are separated by just few Ångströms and the defects are nearly in contact ($\Delta E \sim 12 \text{ eV } \text{\AA}^{-1}$). In case V we find a similar attraction basin, however, the interaction is now stronger (although more short range) and the calculated energy basin has the depth $\Delta E \sim 18 \text{ eV } \text{\AA}^{-1}$.

The present analysis does not demonstrate whether the interaction between the defects is additive or whether the regime is linear. If this is not the case, we say that there is a defect of linearity. For example, we may investigate the possible defect of linearity of the stress field, namely, the difference between the stress field when both defects are present and the sum of the stress fields of the two isolated defects. Let us consider Fig. 9 (bottom panels) where the stress component $\sigma_{zz}(x)$ is measured along the x direction keeping $z=Z_I=Z_C$ (case of horizontal alignment) and for two different relative crack-inclusion distances, namely, ~ 15 nm (left) and ~ 5.5 nm (right). First of all we observe that at the smaller crack-inclusion distance, the stress at the right crack tip decreases. This clearly indicates that the inclusion is able to affect the stress intensification at the tip in agreement with a

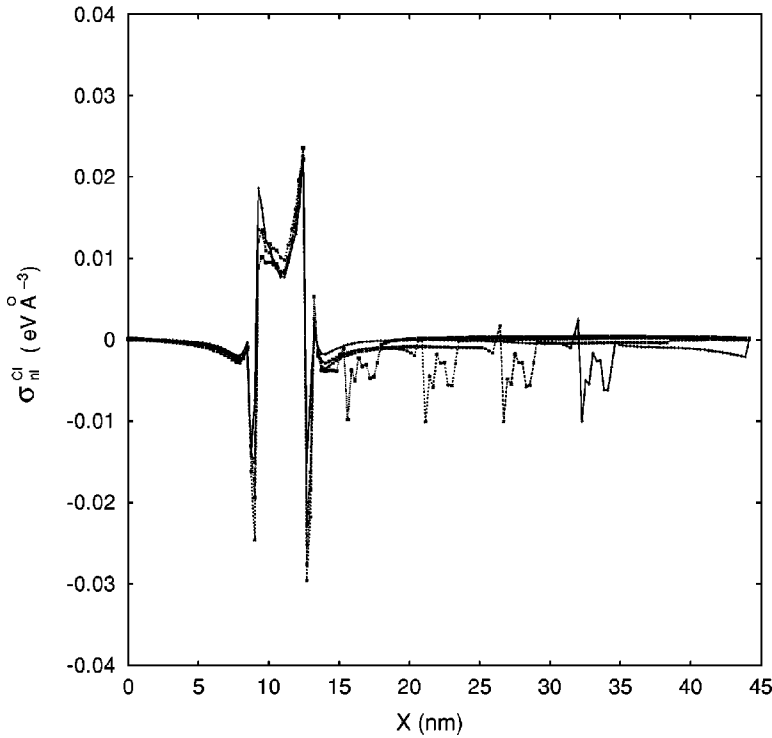


FIG. 10. Defect of linearity $\sigma_{nl}^{CI}(x)$ profiles corresponding to four relative distances d between the crack and the inclusion. Full line: $d=22.2$ nm; long dashed line: $d=16.6$ nm; short dashed line: $d=11.1$ nm; dotted line: $d=5.5$ nm (see text).

possible toughening mechanism. We also prove that such an effect falls beyond the linear regime. Let us define the total stress as the stress that is calculated when both the crack and the inclusion are present in the system. We can compare the total stress with the one calculated in a system containing just one crack or just one inclusion and accordingly define the defect of linearity $\sigma_{nl}^{CI}(x)$ of the zz component of the stress $\sigma_{zz}^{CI}(x)$ as

$$\sigma_{nl}^{CI}(x) = [\sigma_{zz}^{CI}(x) - \sigma_{zz}^{\infty}] - [\sigma_{zz}^C(x) - \sigma_{zz}^{\infty}] - [\sigma_{zz}^I(x) - \sigma_{zz}^{\infty}], \quad (6)$$

where the uniform stress background σ_{zz}^{∞} is subtracted from each contribution (one can define similar quantity for any component of stress and strain, but σ_{zz} is the most relevant for the actual geometry). According to Eq. (6), $\sigma_{nl}^{CI}(x)$ should vanish if the interaction of the two defects is purely additive. Furthermore, $\sigma_{nl}^{CI}(x)$ obviously depends on the relative distance between the two defects. The actual result is presented in Fig. 9 (top panels) and clearly indicates that for an interacting pair of crack inclusion under tensile loading, the mechanical response (stress field) falls beyond the linear regime. At the crack tips the defect of linearity exhibits two negative peaks that tend to reduce the tensile stress. $\sigma_{nl}^{CI}(x)$ actually corresponds to a few percent of the total stress $\sigma_{zz}^{CI}(x)$ when the crack-inclusion distance is small. Such a deviation may not be considered negligible because its role may be relevant near the stress stability threshold of a system containing a crack. Furthermore, its contribution may be important when several crack-inclusion pairs are present in the system.

Let us finally consider the $\sigma_{nl}^{CI}(x)$ profiles corresponding to different relative distances between the crack and the diamond inclusion. If we scale them by a factor depending upon

the relative distance, we find the $\sigma_{nl}^{CI}(x)$ profiles shown in Fig. 10. There we have normalized numerical data so that the height of the peaks at the right tip of the crack were the same. The behavior of $\sigma_{nl}^{CI}(x)$ is represented by a function vanishing everywhere, but for two rather localized regions corresponding to the positions of the crack and the inclusion. Accordingly, we cast the defect of linearity $\sigma_{nl}^{CI}(x)$ in the following form:

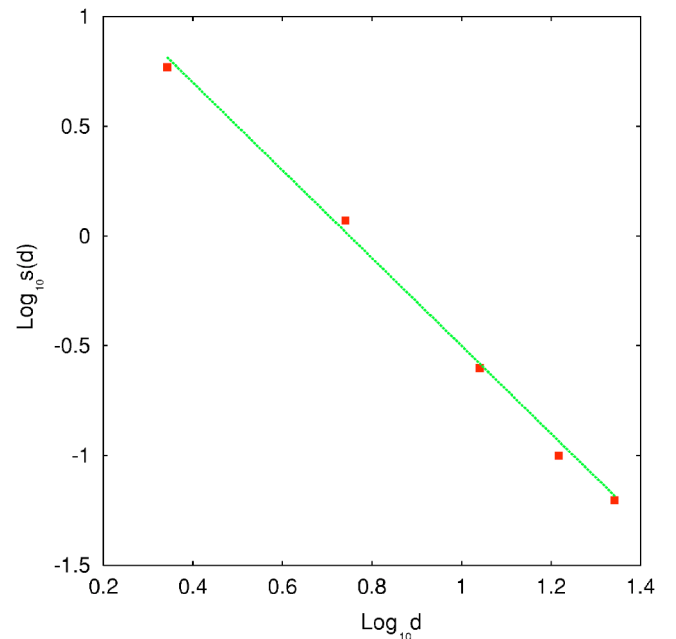


FIG. 11. Scaling function $s(d)$ appearing in Eq. (7) versus relative distance d measured in reduced units $|X_C - X_I|/R$. Points are the scale factors calculated so to get results shown in Fig. 10.

$$\sigma_{nl}^{CI}(x) = s(|X_I - X_C|)[g_C(x - X_C) + g_I(x - X_I)], \quad (7)$$

where $s(|X_I - X_C|)$ is a scaling function only dependent on the relative distance $d = |X_I - X_C|$, while the last factor is the sum of two suitable functions localized at the defect positions. A detailed analysis of the two functions will be presented elsewhere; here we only remark that $g_C(x - X_C)$ exhibits two negative peaks at the crack tips while $g_I(x - X_I)$ is negative in the interior of the inclusion. A plot of the scaling function $s(d)$ versus the distance d shows a power-law behavior as can be verified in Fig. 11, where filled squares represent present data in a log-log plot. Accordingly we can state that the scaling function decays as inverse of the square of the relative distance of the crack and the inclusion $s(|X_I - X_C|) \sim |X_I - X_C|^{-2}$. This leads to an important qualitative result, namely the total stress field can be formulated by means of the following constitutive formulation:

$$\sigma_{zz}^{CI}(x) = \sigma_{zz}^C(x) + \sigma_{zz}^I(x) + \frac{[g_C(x - X_C) + g_I(x - X_I)]}{|X_I - X_C|^2}. \quad (8)$$

This result is one step toward a continuum nonlinear model for the stress of an interacting crack-inclusion couple that is inferred fully from atomistic analysis.

IV. CONCLUSIONS

The interaction between a microcrack and a hard diamond inclusion in β -SiC has been studied by means of molecular dynamics. It has been proved that the basic features of elasticity theory are reproduced even at the atomic scale, both for the crack stress field and for the inclusion displacement field, provided that a renormalization of some basic quantity of continuum theory is suitably defined. By means of a quantitative investigation on the potential energy landscape, we have further demonstrated that at small crack-inclusion distances the elastic energy of the system decreases effectively, i.e., it is energetically more stable. Furthermore the tensile stress at the crack tip decreases due to the presence of the inclusion. Such atomic-scale results are consistent with the possible proposed toughening mechanism according to which the diamond inclusion is able to reinforce the β -SiC crystal. The interaction between the stress fields of the crack and the inclusion has been also investigated in detail; deviation from a simple linear behavior is indeed observed. Finally, it is found that nonlinearity increases according to the inverse of the square of relative distance between the crack tip and the hard inclusion (fiber).

ACKNOWLEDGMENT

This work has been funded by Italian MIUR under P.R.I.N.-2002 project ‘‘Fracture mechanics of complex covalently bonded materials.’’

*Corresponding author. Electronic address:

luciano.colombo@dsf.unica.it

¹J. D. Kuntz, G. Zhan, and A. K. Mukherjee, *Mater. Res. Bull.* **29**, 22 (2004); and references therein.

²K. B. Broberg, *Cracks and Fracture* (Academic Press, San Diego, 1999).

³M. Sahimi, *Heterogeneous Materials II* (Springer-Verlag, Berlin, 2003).

⁴R. L. B. Selinger and D. Farkas, *Mater. Res. Bull.* **25**(5), 11 (2000).

⁵F. Cleri, *Phys. Rev. B* **65**, 014107 (2002).

⁶J. Tersoff, *Phys. Rev. B* **39**, 5566 (1989).

⁷E. Pearson, T. Takai, T. Halicioglu, and W. A. Tiller, *J. Cryst. Growth* **70**, 33 (1984).

⁸F. Shimojo, I. Ebbsjö, R. K. Kalia, A. Nakano, J. P. Rino, and P. Vashishta, *Phys. Rev. Lett.* **84**, 3338 (2000).

⁹M. Tang and S. Yip, *Phys. Rev. Lett.* **75**, 2738 (1995).

¹⁰M. Tang and S. Yip, *Phys. Rev. B* **52**, 15 150 (1995).

¹¹W. Li and T. Wang, *Phys. Rev. B* **59**, 3993 (1999).

¹²M. Tang and S. Yip, *J. Appl. Phys.* **76**, 2719 (1994).

¹³J. Wang, S. Yip, S. R. Phillpot, and D. Wolf, *Phys. Rev. Lett.* **71**, 4182 (1993).

¹⁴J. Wang, J. Li, S. Yip, S. R. Phillpot, and D. Wolf, *Phys. Rev. B* **52**, 12 627 (1995).

¹⁵L. Landau and E. M. Lifshits, *Theory of Elasticity* (Butterworth-Heinemann, Oxford, 1986).

¹⁶F. Cleri, S. R. Phillpot, D. Wolf, and S. Yip, *J. Am. Ceram. Soc. Soc.* **81**, 501 (1998).

¹⁷A. A. Griffith, *Philos. Trans. R. Soc. London London, A* **221**, 163 (1920).

¹⁸We performed careful analysis of the Griffith condition for crack propagation for the present force model and mechanical conditions. The actual values of the crack length and strain guarantee that we are below the Griffith threshold. A more detailed analysis on this issue will be reported elsewhere.

¹⁹B. Pecz, H. Weishart, V. Heera, and L. Toth, *Appl. Phys. Lett.* **82**, 46 (2003).

²⁰J. D. Eshelby, *Proc. R. Soc. London, Ser. A Society London, A* **241**, 376 (1957).